Influence of active layer thickness on the performance of P3HT: $PC_{61}BM$ organic photovoltaic devices analyzed via $J-V$ characteristics

B. Ait Ali and R.Moubah

LPMAT, Faculty of Sciences Ain Chock, Hassan II University of Casablanca, Morocco.
e-mail: brahimaitali30@gmail.com

Received 4 April 2026; accepted 30 April 2026

Optimizing the thickness of the active layer is essential to improve the performance of organic solar cells. In this study, we examined how the thickness of the active layer, made of a P3HT:$PC_{61}BM$ blend, influences the key electrical parameters of inverted organic solar cells. Four prepared photovoltaic cells were prepared using a typical device structure of ITO/ZnO/P3HT:$PC_{61}BM$/MoO_3/Ag. The active layer of P3HT:$PC_{61}BM$ was deposited by spin coating with different thicknesses of 80, 150, 200, and 300 nm. We used the different J–V characteristics to extract parameters such as the open-circuit voltage, short-circuit current density, series resistance, and shunt resistance. Based on these measurements, the results indicate that $V_{\rm oc}$ remains nearly stable between 80 nm and 200 nm, before dropping sharply at 300 nm due to recombination losses. Furthermore, $J_{\rm sc}$ increases with thickness and reaches its maximum at 300 nm, thanks to improved light absorption. The fill factor peaks ($\sim$50%) at a thickness of 150 nm, then decreases, reflecting an imbalance between charge collection and internal losses. To provide a deeper understanding of this behavior, we also analyzed the resistive parameters. The series resistance $R_{\rm s}$ increases from 27.11 $\Omega{\cdot}{\rm m}^2$ to 27.52 $\Omega{\cdot}{\rm m}^2$ when the thickness increases from 80 to 150 nm due to the increased defect density in the layer structure with additional layer stacking, then rises to 28.87–34.55 $\Omega{\cdot}{\rm m}^2$ for 200–300 nm, respectively, because of the longer charge transport path and increased recombination. Finally, the shunt resistance $R_{\rm sh}$ increases up to 150 nm, suggesting improved film uniformity and better surface coverage, thus minimizing shunt defects, before decreasing at 200 and 300 nm. This suggests that increasing the material volume statistically leads to a higher density of volumetric defects.

Keywords: Organic photovoltaic cells; active layer thickness; series resistance; shunt resistance; cell design parameters.

DOI: https://doi.org/10.31349/RevMexFis.72.051003

1. Introduction

The transition to renewable energy sources has become essential in response to growing environmental concerns and the depletion of fossil fuel resources. Among emerging technologies, organic photovoltaics (OPV) have gained increasing attention due to their lightweight nature, mechanical flexibility, potential for low-cost production, and compatibility with large-scale printing processes [1-5]. Unlike traditional silicon-based solar cells, OPVs rely on organic materials, primarily conjugated polymers and small organic molecules to absorb light and generate electricity [6-13]. In recent decades, important advancements have been made in understanding the fundamental mechanisms of photovoltaic conversion in organic materials, as well as in optimizing device architectures. Nevertheless, OPVs still face challenges related to power conversion efficiency and operational stability when compared to their inorganic counterparts. Improving the performance of OPVs requires better control over the optoelectronic properties of the active materials and the optimization of each layer within the device, particularly the active layer and the charge transport layers.

The organic photovoltaic cell is characterized by several key parameters that determine its efficiency in converting light into electrical energy. The first of these parameters is the open-circuit voltage, noted V_{oc}, which represents the maximum voltage the cell can deliver when no current is flowing through the circuit. It is mainly determined by the energy difference between the HOMO level of the donor material and the LUMO level of the acceptor material minus internal energy losses. The second parameter is the short-circuit current density, noted J_{sc}, which corresponds to the amount of current generated when the cell's terminals are directly connected. It depends on the absorption of light, the efficient separation of photogenerated electron-hole pairs, and their collection at the electrodes. Another important parameter is the fill factor (FF), which reflects the quality of the cell's current-voltage ($J-V$) curve. It is defined as the ratio of the maximum power actually delivered by the cell to the theoretical power given by the product $V_{oc} \times J_{sc}$. Finally, the power conversion efficiency, noted PCE, expresses the percentage of the incident light energy that is converted into electricity. In this context, the current work focuses on investigating the effect of the active layer thickness on key performance parameters namely the open-circuit voltage, short-circuit current density, and power conversion efficiency (PCE) of an organic photovoltaic cell based on the P3HT:$PC_{61}BM$ blend. By analyzing the current–voltage ($J-V$) characteristics, the goal is to assess how variations in the active layer thickness influence charge generation, transport, and recombination processes. In addition to the conventional performance metrics, the study also examines the influence of thickness on series resistance (R_s), shunt resistance (R_{sh}). These additional parameters provide deeper insight into the internal physical mechanisms governing device behavior, and help identify the optimal active layer thickness for maximizing photovoltaic performance.

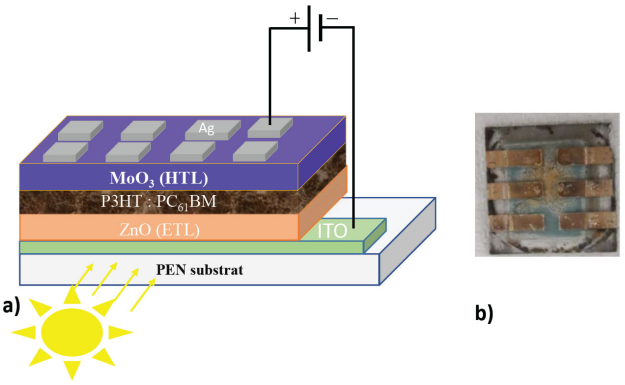

FIGURE 1. a) Schematic illustration of the fabricated OSC with the device architecture of ITO/ZnO/P3HT: $PC_{61}BM$/MoO_3/Ag, and b) photograph of the fabricated device.

2. Experimental details

Here, we describe the fabrication steps of organic solar cells (OSCs). Flexible PEN/ITO substrates (2×2 cm^2, $\leq 15\,\Omega$/sq.) were cleaned in an ultrasonic bath using detergent, acetone, isopropyl alcohol, and deionized water, followed by 30 minutes of UV ozone treatment. ZnO films were deposited by RF magnetron sputtering using a high-purity (99.999%) ZnO target, under an argon atmosphere at a pressure of 10^{-2} mbar, with 100 W power and a substrate temperature of about 40°C, resulting in a thickness of ∼54 nm. Then, PEN/ITO/ZnO samples were annealed in oxygen at temperature 160°C for 1 hour. The active layer was spin-coated using a 1:1 (wt %) P3HT:$PC_{61}BM$ solution in dichlorobenzene, with spin speeds of 3000, 2000, 1800, and 800 rpm to obtain thicknesses of 80, 150, 200, and 300 nm, respectively. The P3HT (98.5% regioregular) and $PC_{61}BM$ were used without further purification [14,15]. After deposition, the samples were annealed at 140°C for 15 minutes in a nitrogen-filled glove box. MoO_3 (5 nm) and Ag (120 nm) were then thermally evaporated under high vacuum (2×10^{-6} Torr) through a shadow mask. The complete device structure (as illustrated in Fig. 1) had an active area of about 9 mm^2. For comparison, the same procedure was applied to rigid ITO-coated PEN substrates (20×20 mm^2, $\leq 20\,\Omega$/sq.).

In brief, the cell layers studied consist of the following constituents:

- **Substrate**: PEN (used as the supporting base for the device structure)
- **Transparent electrode (Anode)**: ITO
- **Electron transport layer (ETL)**: ZnO
- **Photoactive layer**: P3HT:$PC_{61}BM$ blend (poly(3-hexylthiophene) and [6,6]-phenyl-C_{61}-butyric acid methyl ester)
- **Hole transport layer (HTL)**: MoO_3
- **Cathode**: Ag (silver)

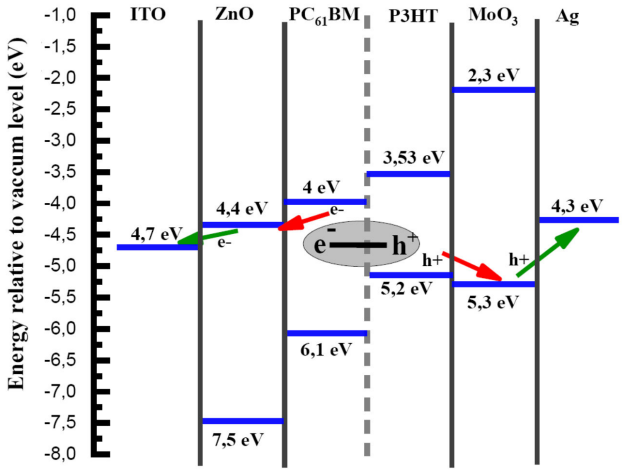

FIGURE 2. Energy levels and charge transport in the studied inverted organic photovoltaic cell.

The energy level diagram of the component materials of the studied inverted P3HT:$PC_{61}BM$ organic solar cells (OSCs) is shown in Fig. 2 [16-20].

Light absorbed in the P3HT component of the P3HT:$PC_{61}BM$ active layer generates excitons through a HOMO–LUMO electronic transition. Due to the strong Coulomb binding in organic semiconductors, these excitons diffuse toward the P3HT/$PC_{61}BM$ interface, where their dissociation is driven by the energy offset between the LUMO levels of the donor and acceptor (Fig. 2). This process results in electron transfer to PCBM while holes remain in P3HT. The free charge carriers are subsequently injected into the charge transport layers, with electrons transported through ZnO and holes through MoO_3, and finally collected at the aluminum cathode and ITO anode to generate the photovoltaic current [14,21-23].

The $J-V$ curves representing current density as a function of voltage of the OSCs were measured using an HP Agilent source measurement unit under simulated illumination. A solar simulator operating under AM 1.5G conditions (Oriel Xenn 150W) was employed. The light intensity was calibrated using a standard silicon solar cell to achieve an illumination of 100 mW/cm^2. Device performance measurements were conducted under a nitrogen atmosphere.

3. Results and discussions

In this case, we execute the standard diode model as expressed in the following analytical Eq. (1) [24,25]:

$$J=J_0\left[\exp\left(\frac{e(V-JR_s)}{nkT}\right)-1\right]+\frac{V-JR_s}{R_{sh}}-J_{ph}, \quad (1)$$

where J_0 and J_{ph} are the diode saturation current density and photocurrent density, R_s and R_{sh} are the series and shunt resistances, n an ideality factor close to 1 indicates bimolecular recombination, while a value near 2 suggests trap-assisted or

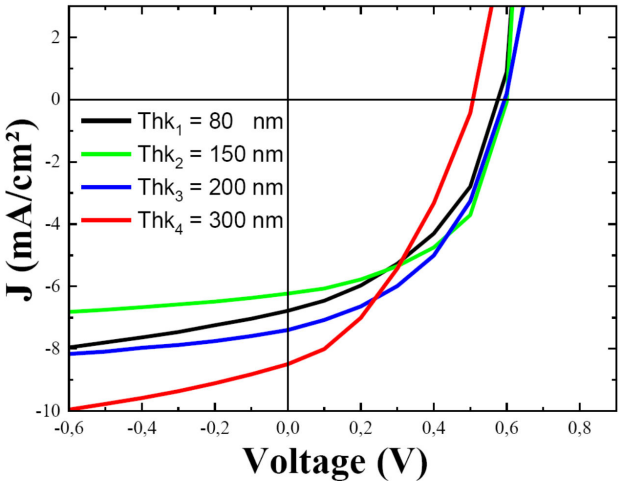

FIGURE 3. Current density-voltage response of P3HT: $PC_{61}BM$ devices as a function of the active layer thickness.

interface recombination, e, k, and T represent the elementary charge, the Boltzmann constant, and the absolute temperature, respectively; and V the applied voltage. The $J-V$ curves of the organic solar cells (OSCs) with different active layer thicknesses were displayed in Fig. 3. The current–voltage ($J-V$) characteristics of organic solar cells (OSCs) were measured as a function of active layer thickness. The results show that thickness strongly affects device efficiency. An OSC with an 80 nm active layer exhibits a short-circuit current density (J_{sc}) of 6.8 mA/cm^2, an open-circuit voltage (V_{oc}) of 0.57 V, and an efficiency (η) of 1.7%. Increasing the thickness to 150 nm slightly reduces J_{sc} to 6.3 mA/cm^2, while V_{oc} improves to 0.60 V, leading to the highest PCE of 1.9%. Further increasing the thickness to 300 nm degrades V_{oc} and overall efficiency, despite a slight increase in J_{sc}.

The influence of the active layer thickness on the photovoltaic performance was investigated by analyzing the evolution of the open-circuit voltage (V_{oc}), short-circuit current density (J_{sc}), fill factor (FF), series resistance (R_s), shunt resistance (R_{sh}), and efficiency (η) as a function of thickness. The performance parameters of the devices corresponding to the $J-V$ curves are listed in Table I, in which it clearly appears that the active layer thickness has a significant impact on device efficiency.

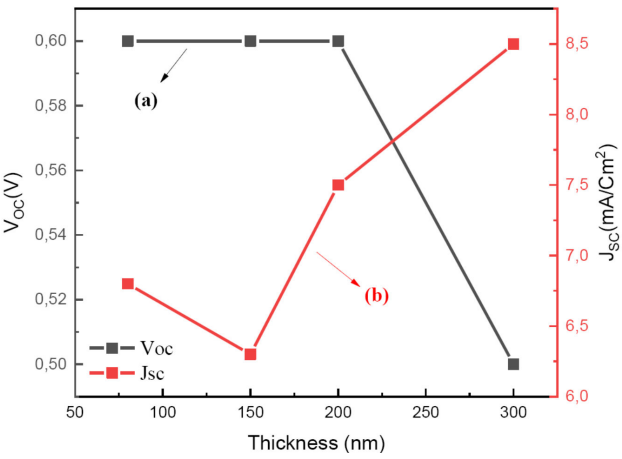

FIGURE 4. a) Open-circuit voltage (V_{OC}) and b) short-circuit current density (J_{SC}) of P3HT:$PC_{61}BM$ solar cells versus active layer thickness.

As presented in Fig. 4a), the open-circuit voltage (V_{oc}) remains almost constant at around 0.60 V for active layer thicknesses ranging from 80 nm to 200 nm. However, a significant decrease is observed when the thickness reaches 300 nm. This reduction in V_{oc} at greater thickness leads to an increase in energy loss, defined as $E_{\text{loss}} = E_g - eV_{oc}$, where E_g is the optical band gap of P3HT:$PC_{61}BM$ ($E_g = 1.9$ eV) [26]. For devices with active layers between 80 and 200 nm, V_{oc} was maintained at 0.6 V, corresponding to an energy loss of about 1.3 eV. When the thickness increases to 300 nm, E_{loss} rises to 1.4 eV. This increase in energy loss is attributed to enhanced non-radiative recombination , which reduces the open-circuit voltage and leads to higher energy dissipation, factors that directly influence V_{oc}, as described by Eq. (2) [21,27,28]:

$$V_{oc} = \frac{E_g}{e} - \frac{kT}{e} \ln\left(\frac{(1-P)(B_L + B_{SRH})N_{CV}^2}{PG}\right), \quad (2)$$

where E_g denotes the effective bandgap of the active layer, P represents the exciton dissociation probability (exciton = (electron–hole) pairs), N_{CV} is the effective density of states, while G is the generation rate of excitons; B_L and B_{SRH} are the strengths of Langevin and Shockley-Read - Hall (SRH) recombination, respectively [29]. As described in Eq. (2), the increase in energy loss in thicker active layer devices is mainly due to higher charge recombination. When the thickness increases, charge carriers displace longer distances, which increases the probability of bimolecular (BL) and Shockley-Read-Hall (SRH) recombination before reaching the electrodes. This reduces the number of collected free charges and increases energy losses. In contrast, the short-circuit current density (J_{sc}) observed in Fig. 4b) increases steadily with increasing active layer thickness, reaching its maximum value at 300 nm. This trend is expected since thicker layers absorb more incident light, generating more charge carriers [27]. However, beyond a certain thickness, the recombination losses may offset the gain in light absorption. The fill factor (FF), shown in Fig. 5a), reaches its maximum (∼50%) at around 150 nm, then decreases with further increases in thickness. This behavior suggests that an optimal thickness exists where the internal resistance is minimized and charge collection is most efficient. Thinner layers may suffer from insufficient absorption, while thicker layers may introduce transport limitations [21,27,30,31]. Studies have shown that the distribution of excitons affects charge transport and collection due to the mobility and transport distance of the carriers [32-34].

Generally, an active layer thickness around 150-200 nm appears to provide a good balance between light absorption and charge collection, leading to optimal device performance. At 300 nm, although J_{sc} is maximized, the simultaneous drop

TABLE I. Photovoltaic parameters of P3HT: $PC_{61}BM$ BHJ OSCs with different active layer thickness under AM 1.5 G solar illumination.

Active layer thickness	V_{oc} (V)	J_{sc} (mA/cm^2)	FF (%)	Efficiency (η %)	R_s (Ω·cm^2)	R_{sh} (Ω·cm^2)
80 nm	0.57	6.8	42.3	1.7	27.11	307.76
150 nm	0.60	6.3	50.4	1.9	27.52	621.38
200 nm	0.59	7.5	44.1	2.0	28.87	306.82
300 nm	0.50	8.5	37.1	1.6	34.55	206.23

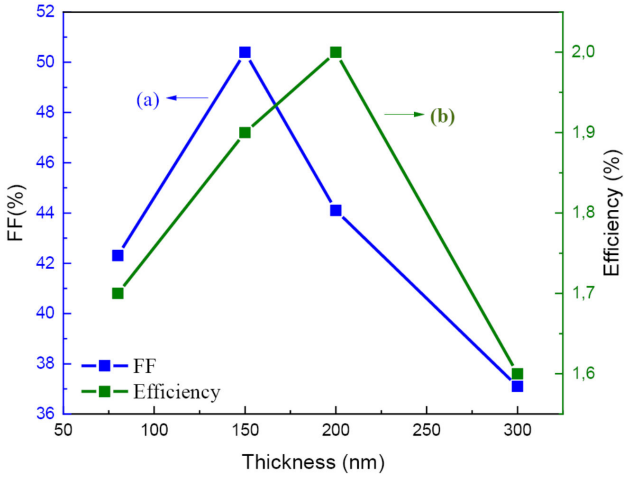

FIGURE 5. a) Fill factor, b) Efficiency (%) of P3HT: $PC_{61}BM$ solar cells as a function of the active layer thickness.

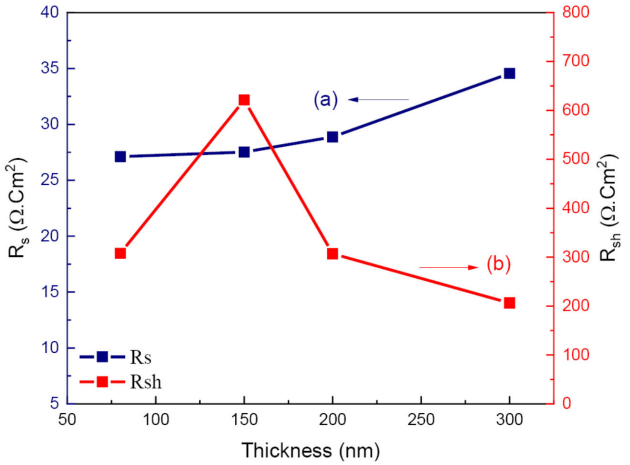

FIGURE 6. Variation of a) series resistance (R_s) and b) shunt resistance (R_{sh}) with active layer thickness in P3HT:$PC_{61}BM$ solar cells.

in V_{oc} and FF likely results in a reduced overall power conversion efficiency. The parasitic resistances are derived from the $J(V)$ curve: the series resistance R_s is the inverse of the slope near the V_{oc} point, while the shunt resistance R_{sh} is the inverse of the slope near the J_{sc} point [35]. These values are crucial for assessing performance losses, using linear fits the obtained values were displayed in Table I.

The series resistance R_s values are illustrated in Fig. 6a) (The obtained values are of the same order of magnitude as those reported by other researchers for organic photovoltaic cells [7,30]. We observed that the series resistance increases with thickness [see Fig. 6a)]. However, the main factors limiting the performance of devices with a thicker $PC_{61}BM$:P3HT active layer lie in the low electron mobility within the active layer, caused by the increased defect density in the material structure with additional layer stacking, as well as the reduced charge collection efficiency at the electrodes, since holes and electrons recombine before reaching the electrodes, rather than in the increase of R_s itself [21,27,30]. The values of R_{sh} were shown in Fig. 6b). The shunt resistance value was found to be 307.76 Ω·cm^2 for the 80 nm thickness and 621.38 Ω·cm^2 for the 150 nm thickness. The shunt resistance increases significantly. In this range, the initial increase in active layer thickness may lead to improved film uniformity and better surface coverage, thereby reducing the density of short-circuited regions and leakage paths (shunt defects) created during deposition. Then, the shunt resistance value decreases to 606.81 $\Omega\cdot$ cm^2 at 200 nm and 206.23 Ω·cm^2 at 300 nm.

When the active layer becomes excessively thick (beyond 150 nm), the number of bulk defects increases, the larger volume of material statistically increases the total number of defects (pores, agglomerates, and impurities) [30].

The optimal active layer thickness for the cell under study was found to be 150 nm. This choice represents the best compromise, as it allows the maximization of shunt resistance R_{sh} (which minimizes leakage current losses) while keeping the series resistance R_s at a low value, thus ensuring an optimized overall performance of the cell. For the efficiency η presented in Fig. 5b), we observe that when the thickness of the active layer in a photovoltaic cell increases, the ability to absorb light improves, which enhances the generation of electrical charges and thus the efficiency [36]. However, beyond a certain thickness (here 300 nm), negative effects start to dominate: the generated charges have more difficulty reaching the electrodes, which increases recombination because the charges neutralize before producing current. This reduces the overall efficiency of the cell.

4. Conclusions

In summary, we have explored how varying the active layer thickness affects the photovoltaic response of P3HT:$PC_{61}BM$ polymer solar cells. The results show that V_{oc} remains almost constant between 80 nm and 200 nm, then drops significantly at 300 nm, indicating increased recombination losses. J_{sc} increases steadily with thickness, reaching a maximum

at 300 nm due to improved light absorption. The fill factor reaches its peak ($\sim$50%) at 150 nm and then decreases, reflecting a balance shift between charge collection and internal losses.

Our results show that the active layer thickness strongly affects R_s and R_{sh}: an optimal value around 150 nm minimizes defects, improves film quality, and enhances charge transport, leading to better photovoltaic performance. These results demonstrate that the thickness of the active layer has a complex yet critical influence on the overall performance of organic solar cells, and that an optimal compromise must be found between light absorption, charge transport, and recombination.

1. T. Yang *et al*., Inverted polymer solar cells with a solution-processed zinc oxide thin film as an electron collection layer, *Sci. China Chem.* **55** (2012) 755, https://doi.org/10.1007/s11426-012-4512-2
2. L. Dou *et al*., Tandem polymer solar cells featuring a spectrally matched low-bandgap polymer, *Nature Photon* **6** (2012) 180, https://doi.org/10.1038/nphoton.2011.356
3. S. Saha and N. B. Manik, Enhancement of efficiency of Phenosafranin based organic photovoltaic devices using nano particles, *Indian J. Phys.* **86** (2012) 605, https://doi.org/10.1007/s12648-012-0090-6
4. F. Rehman *et al*., Developing small molecule-based donor materials for organic solar cells: a DFT/TD-DFT insight, *Indian J Phys* **99** (2025) 3915, https://doi.org/10.1007/s12648-025-03575-3
5. Y. Gündoğdu, Third-order nonlinear optical properties of fullerene C60 in organic solvents using femtosecond laser zscan, *Indian J Phys* **97** (2023) 915, https://doi.org/10.1007/s12648-023-02612-3
6. B. Ait Ali *et al*., Charge Transport and Photovoltaic Properties of Conjugated Polymer PTB7:PC71BM Based Solar Cells, *Trans. Electr.* Electron. Mater. **21** (2020) 436, https://doi.org/10.1007/s42341-020-00198-9
7. A. Jouane *et al*., Morphological and micro-structural interface characterization in multilayer inverted polymer-fullerene bulk heterojunction solar cells, *Solar Energy Materials and Solar Cells* **180** (2018) 258, https://doi.org/10.1016/j.solmat.2017.06.044
8. B. Ait Ali *et al*., Temperature-dependent barrier height inhomogeneities in PTB7:PC71BM-based organic solar cells, *Chinese Phys. B* **29** (2020) 098801, https://doi.org/10.1088/1674-1056/aba5fc
9. J. J. M. Halls *et al*., Efficient photodiodes from interpenetrating polymer networks, *Nature* **376** (1995) 498, https://doi.org/10.1038/376498a0
10. G. Yu *et al*., Polymer Photovoltaic Cells: Enhanced Efficiencies via a Network of Internal Donor-Acceptor Heterojunctions, *Science* **270** (1995) 1789, https://doi.org/10.1126/science.270.5243.1789
11. P. K. Das, S. Sen, and N. B. Manik, Study on the series resistance of crystal violet dye-based organic photovoltaic device in presence of single walled carbon nanotubes, *Indian J Phys* **96** (2022) 1423, https://doi.org/10.1007/s12648-021-02051-y
12. M. Sharma *et al*., Organic photodiode based on PTB7-Th:PCBM as photoactive layer, *Indian J Phys* **100** (2026) 713, https://doi.org/10.1007/s12648-025-03780-0
13. D. Gogoi, S. Bhattarai, and T. D. Das, Influence of altered parasitic aspects on the device structure for efficient organic solar cells, *Pramana - J Phys* **97** (2023) 188, https://doi.org/10.1007/s12043-023-02660-8
14. A. K. K. Kyaw *et al*., An inverted organic solar cell employing a sol-gel derived ZnO electron selective layer and thermal evaporated MoO3 hole selective layer, *Applied Physics Letters* **93** (2008) 221107, https://doi.org/10.1063/1.3039076
15. D. Gogoi, S. Bhattarai, and T. D. Das, A numerical investigation for performance enhancement of organic solar cell using Al-doped zinc oxide anode, *Indian J Phys* **98** (2024) 2705, https://doi.org/10.1007/s12648-023-03042-x
16. Y. Min Nam, J. Huh, and W. Ho Jo, Optimization of thickness and morphology of active layer for high performance of bulk-heterojunction organic solar cells, *Solar Energy Materials and Solar Cells* **94** (2010) 1118, https://doi.org/10.1016/j.solmat.2010.02.041
17. L. Ma *et al*., A ternary organic solar cell with 300 nm thick active layer shows over 14% efficiency, *Sci. China Chem.* **63** (2020) 21, https://doi.org/10.1007/s11426-019-9556-7
18. K. Liu *et al*., Wrinkled substrate and Indium Tin Oxide-free transparent electrode making organic solar cells thinner in active layer, *Journal of Power Sources* **331** (2016) 43, https://doi.org/10.1016/j.jpowsour.2016.09.038
19. G. Zhang *et al*., Active emitting layer thickness dependence and interfaces engineering studies on the performance of DOPPP white organic light emitting diodes, *Optics Communications* **459** (2020) 124921, https://doi.org/10.1016/j.optcom.2019.124921
20. O. Dhibi *et al*., Inverted low band gap polymer solar cells integrated with a low-temperature-annealed sol-gel-derived ZnO: Active layer thickness effect on the recombination process, *Superlattices and Microstructures* **60** (2013) 548, https://doi.org/10.1016/j.spmi.2013.05.032
21. G. Namkoong *et al*., Active layer thickness effect on the recombination process of PCDTBT:PC71BM organic solar cells, *Organic Electronics* **14** (2013) 74, https://doi.org/10.1016/j.orgel.2012.10.025

22. Q. Zhang *et al*., Inverted Organic Solar Cells with Low- Temperature Al-Doped-ZnO Electron Transport Layer Processed from Aqueous Solution, *Polymers* **10** (2018) 127, https://doi.org/10.3390/polym10020127

23. D. Salem *et al*., Ag nanoparticle-based efficiency enhancement in an inverted organic solar cell, *Eur. Phys. J. Appl. Phys.* **90** (2020) 30201, https://doi.org/10.1051/epjap/2020200112

24. S. Hwang and T. Yasuda, Indoor photovoltaic energy harvesting based on semiconducting π-conjugated polymers and oligomeric materials toward future IoT applications, *Polym J* **55** (2023) 297, https://doi.org/10.1038/s41428-022-00727-8

25. I. Houiji *et al*., Modeling and optimization of organic tandem photovoltaic solar cells using silver nanowires as electrode and interconnecting layer, *Eur. Phys. J. Appl. Phys.* **93** (2021) 20202, https://doi.org/10.1051/epjap/2021200354

26. P. R. Berger and M. Kim, Polymer solar cells: P3HT:PCBM and beyond, *Journal of Renewable and Sustainable Energy* **10** (2018) 013508, https://doi.org/10.1063/1.5012992

27. Y. Zang *et al*., Effect of Active Layer Thickness on the Performance of Polymer Solar Cells Based on a Highly Efficient Donor Material of PTB7-Th, *J. Phys. Chem. C* **122** (2018) 16532, https://doi.org/10.1021/acs.jpcc.8b03132

28. H. Yao *et al*., Design, Synthesis, and Photovoltaic Characterization of a Small Molecular Acceptor with an Ultra-Narrow Band Gap, *Angew Chem Int Ed* **56** (2017) 3045, https://doi.org/10.1002/anie.201610944

29. M. Kuik *et al*., Determination of the trap-assisted recombination strength in polymer light emitting diodes, *Applied Physics Letters* **98** (2011) 093301, https://doi.org/10.1063/1.3559911

30. N. Sharma, S. K. Gupta, and C. M. Singh Negi, Influence of active layer thickness on photovoltaic performance of PTB7:PC70BM bulk heterojunction solar cell, *Superlattices and Microstructures* **135** (2019) 106278, https://doi.org/10.1016/j.spmi.2019.106278

31. J. Mescher *et al*., Illumination angle and layer thickness influence on the photo current generation in organic solar cells: A combined simulative and experimental study, *AIP Advances* **5** (2015) 077188, https://doi.org/10.1063/1.4928074

32. Y. Zang *et al*., Improved performance of polymer solar cells using PBDTT-F-TT:PC 71 BM blend film as active layer, *Applied Surface Science* **376** (2016) 138, https://doi.org/10.1016/j.apsusc.2016.03.080

33. J. Zou *et al*., High-Performance Inverted Polymer Solar Cells: Device Characterization, Optical Modeling, and Hole-Transporting Modifications, *Adv. Funct. Materials* **22** (2012) 2804, https://doi.org/10.1002/adfm.201102937

34. T. Kobori and T. Fukuda, Effect of optical intensity distribution on device performances of PTB7-Th:PC71BM-based organic photovoltaic cells, *Organic Electronics* **51** (2017) 76, https://doi.org/10.1016/j.orgel.2017.09.006

35. A. El Karkri *et al*., Characterization and simulation study of organic solar cells based on donor-acceptor (D-π-A) molecular materials, *RSC Adv.* **10** (2020) 18816, https://doi.org/10.1039/D0RA01815E

36. D. Zhang *et al*., Recent progress in thick-film organic photovoltaic devices: Materials, devices, and processing, *SusMat* **1** (2021) 4, https://doi.org/10.1002/sus2.10